

Full Length Article

The origin of the enhanced photoresponsivity of the phototransistor with $\text{ZnO}_{1-x}\text{S}_x$ single active layer

Jong Hun Yu^{a,b,1}, Woo-Jung Lee^{a,c,1}, Dae-Hyung Cho^{a,c}, Woo-Ju Kim^{a,c}, Seong Jun Kang^{b,*},
Yong-Duck Chung^{a,c,*}

^a ICT Creative Research Laboratory, Electronics and Telecommunications Research Institute, Daejeon 34129, Republic of Korea

^b Department of Advanced Materials Engineering for Information and Electronics, Kyung Hee University, 1732 Deogyong-daero, Giheng-gu, Yongin, Gyeonggi-do 17104, Republic of Korea

^c Department of Advanced Device Technology, Korea University of Science and Technology, Daejeon 34113, Republic of Korea



ARTICLE INFO

Keywords:

Oxide semiconductor thin-film transistor
 $\text{ZnO}_{1-x}\text{S}_x$
Photoresponsivity
Oxygen vacancy

ABSTRACT

We applied zinc oxysulfide ($\text{ZnO}_{1-x}\text{S}_x$) as a single active layer in a phototransistor by adjusting the S-to-O ratio. The electrical properties and photoresponsivity of the phototransistors were investigated as a function of the S content, x , of the $\text{ZnO}_{1-x}\text{S}_x$ active layer. The incorporation of S atoms in the $\text{ZnO}_{1-x}\text{S}_x$ layer induced a change in the electrical properties and photoresponsivity, especially in the ultraviolet (UV) and visible regions, compared with a ZnO film. The phototransistor with $\text{ZnO}_{0.9}\text{S}_{0.1}$ showed the highest performance; for 450 nm light, the photoresponsivity was 8.0×10^2 A/W, and the maximum photosensitivity was 1.7×10^4 . By analyzing the chemical states of $\text{ZnO}_{1-x}\text{S}_x$ in the phototransistor, we realized that the origin of the improvement of the photoresponsivity is due to the increase of the number of oxygen vacancies formed by the incorporation of S atoms. Based on the above results, we suggested the mechanism of electron transport in phototransistors with a $\text{ZnO}_{1-x}\text{S}_x$ active layer as a function of S content using band alignment. Consequently, we successfully demonstrated the feasibility of the $\text{ZnO}_{1-x}\text{S}_x$ film as a single active layer in a phototransistor to enhance the photoresponsivity in the UV and visible regions.

1. Introduction

In the advent of the Internet of Things era, users can instantly receive information through electronic devices from anywhere [1–3]. As photosensors recognize objects and allow users to communicate with electronic devices, the importance of photosensors has continuously increased [4,5]. Photosensors are already being used in various fields, such as healthcare, optoelectronics, and information technology [6,7]. Among them, thin-film transistors (TFTs) using oxide semiconductors are considered promising photosensors because of their high field-effect mobility, stability, transparency, low leakage current, and their availability in large-scale devices [8–10].

Zinc oxide (ZnO) is a conventional material used in oxide semiconductor TFTs [11,12]. Advanced studies have been conducted on oxide phototransistors with ZnO as the active layer, including for stretchable devices and higher photoresponsivity [13,14]. Phototransistors with a ZnO active layer show poor photoresponsivity in the

visible light region because of its wide band gap [15]. To improve the photoresponsivity in the visible light region, heterostructures with small band gap materials, such as two-dimensional semiconductors, metal nanoparticles, and organic semiconductors, have been used [16–18]. However, these heterostructures led to the formation of interfacial traps and an increase in the off-current in the phototransistor [19,20]. These factors resulted in poor performance and instability of the device [21–23]. Ultimately, heterostructures with other materials required additional processing [24]. Thus, it is necessary to form a single active layer in phototransistors, satisfying both high photoresponsivity in the visible light region and good performance as a phototransistor.

Zinc oxysulfide ($\text{ZnO}_{1-x}\text{S}_x$) is often used in photovoltaic devices because of its stability, wide band gap, and nontoxicity [25–27]. In addition, $\text{ZnO}_{1-x}\text{S}_x$ has tunable electronic properties, achieved by adjusting the S-to-O ratio [28,29]. There are several deposition techniques for the formation of $\text{ZnO}_{1-x}\text{S}_x$ films, such as reactive sputtering, atomic layer deposition, and chemical bath deposition [30,31]. In the

* Corresponding authors.

E-mail addresses: junkang@khu.ac.kr (S. Jun Kang), ydchung@etri.re.kr (Y.-D. Chung).

¹ J. H. Y. and W.-J. L. contributed equally to this work.

reactive sputtering method, using a ZnS single target, the S-to-O ratio in ZnO_{1-x}S_x can be easily adjusted by controlling the O₂/Ar mixed gas flux [32–34]. Variation in the energy level and band gap bowing behavior of ZnO_{1-x}S_x typically occur [35,36]. When S/(S + O) is less than 0.5, the band gap of ZnO_{1-x}S_x decreases as S/(S + O) increases [37,38].

In this study, we applied ZnO_{1-x}S_x with *x* contents of 0, 0.1, and 0.2 as the single active layer of a phototransistor to verify the feasibility of the ZnO_{1-x}S_x film. The band gap of ZnO_{1-x}S_x decreased as the amount of S increased. Phototransistors with ZnO_{0.9}S_{0.1} exhibited the best performance with respect to the threshold voltage and subthreshold swing. The presence of S atoms (*x* ~ 0.1) improved the photoresponsivity under illumination in both the ultraviolet (UV) and visible regions. The photoresponsivity and maximum photosensitivity were 8.0 × 10² A/W and 1.7 × 10⁴ under 450 nm light illumination. From the X-ray photoelectron spectroscopy (XPS) results, we discovered that the number of oxygen vacancies increased with increasing S content in the ZnO_{1-x}S_x film, resulting in an improvement in the photoresponsivity. Moreover, the mechanism of electron transport was suggested through energy band alignment in phototransistors with ZnO_{1-x}S_x as a function of S content. The incorporation of S atoms in ZnO_{1-x}S_x induced a decrease in the band gap and the formation of sub-gaps within the band gap, which allows the formation of oxygen vacancies simultaneously. When light in the UV and visible regions is injected into the phototransistor, the probability of electron excitation is increased in proportion to the S content, resulting in the improvement of photoresponsivity. However, the incorporation of S atoms in ZnO_{1-x}S_x deteriorated the mobility of electrons, reducing the number of electrons that could contribute to the current. Thus, the photoresponsivity of the phototransistor was the best in the case of ZnO_{0.9}S_{0.1}. Consequently, we confirmed that we successfully applied a ZnO_{1-x}S_x single active layer to a phototransistor with improved photoresponsivity in the UV and visible regions.

2. Experimental section

2.1. Device fabrication

Si/SiO₂ wafer (thickness of SiO₂ = 100 nm) was cleaned by sonication using acetone, isopropyl alcohol, and deionized water. A ZnO_{1-x}S_x layer was deposited by reactive sputtering with a single ZnO or ZnS sputter target, adjusting the working pressure and the O₂ pure gas flux or O₂/Ar (10 %) mixed gas flux at a substrate temperature of 300 °C, respectively [29,30]. The thickness of the ZnO_{1-x}S_x was approximately 20 nm. The working pressure of ZnO was 30 mTorr, and O₂/(O₂ + Ar) was 25.0 %. In the case of ZnO_{0.9}S_{0.1}, the working pressure was 5 mTorr, and O₂/(O₂ + Ar) was 3.0 %. For ZnO_{0.8}S_{0.2}, the working pressure was 5 mTorr, and O₂/(O₂ + Ar) was 1.8 % [32–34]. Finally, an Al electrode was deposited at 100 nm through e-beam evaporation.

2.2. Characterization

The transfer curves of the phototransistors were characterized using a semiconductor parameter analyzer (HP 4145B, HP, USA) and a probe station. The optoelectrical characteristics under dark condition and various illumination with the wavelengths (λ) of 405, 450, 535, and 650 nm were investigated with an illumination power of approximately 4.5 mW/cm² (CPS520, Thorlabs, USA) [14,39–41]. The optical transmittance was measured using an ultraviolet–visible (UV–vis) spectrophotometer (Lambda 1050, PerkinElmer, USA). XPS measurements (PHI 5000 VersaProbe, Ulvac-PHI, Japan) were performed to analyze the interfacial chemical properties of the phototransistors with an Al Kα (1486.6 eV) source.

2.3. Composition of ZnO_{1-x}S_x film

The composition of the ZnO_{1-x}S_x film was determined by the ratio of S to O, derived from the XPS atomic concentration results.

3. Results and discussion

Fig. 1a shows the optical transmittance of the ZnO_{1-x}S_x film with the varied S content. The average transmittance between 400 and 700 nm was measured of 99.1 % for ZnO, 97.0 % for ZnO_{0.9}S_{0.1}, and 95.0 % for ZnO_{0.8}S_{0.2}. All cases showed high transparency in the visible region. Fig. 1b shows the tauc plot of ZnO_{1-x}S_x as a function of S content obtained from optical transmittance by calculating the absorption coefficient [36,37].

$$(\alpha \hbar \nu)^2 = \left(\frac{2.303A}{t} \times \frac{\hbar \nu c}{\lambda} \right)^2 = \left\{ \frac{2.303(2 - \log_{10} T)}{t} \times \frac{\hbar \nu c}{\lambda} \right\}^2$$

The extrapolation technique was used to confirm the band gap of ZnO_{1-x}S_x [29,32,33]. The band gap was measured of 3.24 eV for ZnO, 3.15 eV for ZnO_{0.9}S_{0.1}, and 2.96 eV for ZnO_{0.8}S_{0.2}. As the amount of S increased, the band gap values of ZnO_{1-x}S_x decreased, which implies that the ZnO_{1-x}S_x film can be used as a replacement for ZnO in phototransistors in terms of optical properties.

We therefore fabricated phototransistors with a ZnO_{1-x}S_x single active layer as a function of S content. Fig. 2a shows the phototransistor structure. A 100 nm-thick SiO₂ layer was formed on a p⁺⁺ Si wafer through the oxidation process. When a voltage higher than the threshold voltage is applied to the Si gate, an accumulation region is formed in the ZnO_{1-x}S_x active layer, and a channel is created. The current can flow between the Al source and drain through this channel [42,43]. Phototransistors exhibited various photoelectric properties according to the wavelength of the incident light. The transfer curves of the phototransistors with the ZnO_{1-x}S_x active layer under dark conditions are shown in Fig. 2b. The drain voltage (V_D) was 20 V, and the gate voltage (V_G) was varied from –30 V to 30 V. As the amount of S increased, the maximum value of the on-current decreased. Additionally, the shape of the transfer curve became unstable as the amount of S increased, which indicates the deterioration of the electrical properties of the phototransistor. Four parameters were calculated for the dark transfer curves, as summarized in Table 1. μ(sat) is electron saturation mobility. V_{th} is threshold voltage, which is the voltage required to create a conductive path in the active layer. Subthreshold swing is the voltage required to increase the current 10 times. I_{on}/I_{off} is the on–off ratio, which is the on-current divided by the off-current. Interestingly, we observed that the threshold voltage and subthreshold swing were the best in the phototransistor with ZnO_{0.9}S_{0.1}, whereas a hump-like shape appeared in the case of ZnO_{0.8}S_{0.2}, as indicated by the black arrow in Fig. 2b, which indicates a significant deterioration of the electrical properties. When the S content was more than half of the composition of ZnO_{1-x}S_x, the phototransistor did not operate (Supporting Fig. S1). Electrical properties such as electron saturation mobility and on–off ratio significantly deteriorated with increasing S content. It is explained by the change in the atomic lattice derived from the incorporation of S into the ZnO lattice, which interferes with the movement of electrons and leads to the scattering of electrons [36]. Thus, it resulted in poor performance of phototransistors with a ZnO_{1-x}S_x (*x* > 0.2) active layer.

The transfer curves of the phototransistors with the ZnO_{1-x}S_x active layer were measured to evaluate the characteristics of photoresponsivity according to the wavelength. Fig. 3 shows the photoelectrical properties of the phototransistors with the ZnO_{1-x}S_x active layer under various illumination (λ = 635 nm, 535 nm, 450 nm, and 405 nm; power density = 4.5 mW/cm²). The V_D was 20 V, and the V_G was set from –30 V to 30 V. Transfer curves of the phototransistors with ZnO can be confirmed by Fig. 3a. Because the band gap of ZnO was 3.24 eV, the phototransistor with the ZnO active layer responds to UV light of 405 nm, and the photocurrent is generated by the migration of electrons from the valence band to the conduction band of ZnO. However, increased photocurrent and negative shifts of the threshold voltage were found in light of 450 nm and 535 nm, which may be due to the existence of oxygen vacancies formed at the sub-gaps within ZnO [44–46]. Ionized oxygen vacancies

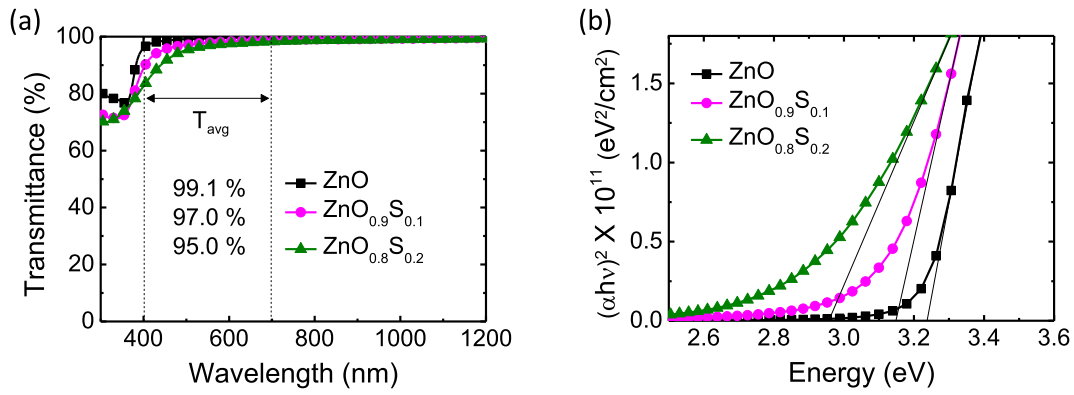


Fig. 1. (Color online) (a) Transmittance of ZnO_{1-x}S_x film. (b) Tauc plot of ZnO_{1-x}S_x film.

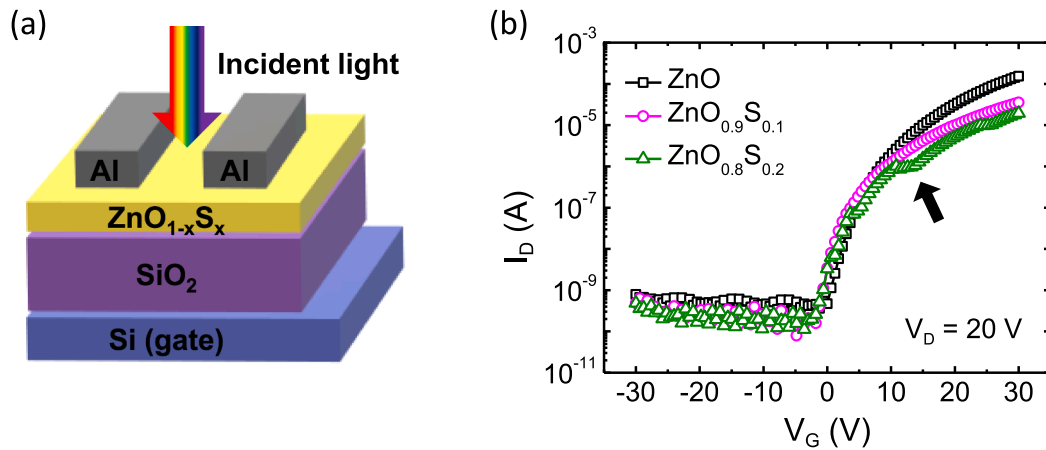


Fig. 2. (Color online) (a) Schematic design of the phototransistors with ZnO_{1-x}S_x single active layer. (b) Transfer curves of the phototransistors with ZnO_{1-x}S_x single active layer without illumination.

Table 1

Four electrical parameters calculated from the dark transfer curves of ZnO_{1-x}S_x in Fig. 2b. $\mu(\text{sat})$ is electron saturation mobility. V_{th} is threshold voltage, which is the voltage required to create a conductive path in the active layer. Subthreshold swing is the voltage required to increase the current 10 times. $I_{\text{on}}/I_{\text{off}}$ is the on-off ratio, which is the on-current divided by the off-current.

	$\mu(\text{sat})$ (cm ² /V·s)	V_{th} (V)	Subthreshold Swing (V ⁻¹)	$I_{\text{on}}/I_{\text{off}}$
ZnO	0.189	12.9	1.455	3.133×10^5
ZnO _{0.9} S _{0.1}	0.054	10.1	0.917	1.468×10^5
ZnO _{0.8} S _{0.2}	0.035	14.7	1.503	0.866×10^5

by an electric field or illumination acts as a donor to generate a photocurrent, even for light with low energy [47,48]. Fig. 3b shows the transfer curves of the phototransistor with ZnO_{0.9}S_{0.1}. The photoresponsivity improved in both the UV and visible light regions. The improvement was significantly greater for the light of 405 nm and 450 nm. The band gap of ZnO_{0.9}S_{0.1} was 3.15 eV, smaller than that of ZnO. Additionally, the incorporation of S into the ZnO lattice induces the formation of oxygen vacancies [49,50]. We deduced that these factors contribute to the improved photoresponsivity of the phototransistor with ZnO_{0.9}S_{0.1} in both the UV and visible light regions. When the transfer curves of the phototransistor with ZnO_{0.8}S_{0.2} are investigated, as shown in Fig. 3c, the photoresponsivity was higher than that of ZnO, but not higher than that of ZnO_{0.9}S_{0.1}. Moreover, the transfer curves in

Fig. 3c are entirely unstable. The band gap of ZnO_{0.8}S_{0.2} was 2.96 eV, smaller than that of ZnO_{0.9}S_{0.1}, and ZnO_{0.8}S_{0.2} has more oxygen vacancies because of the increased amount of S. Then the phototransistor with ZnO_{0.8}S_{0.2} was expected to have a higher photoresponsivity than that with ZnO_{0.9}S_{0.1}, but it was not. We could affirm that an excessive amount of S in the ZnO lattice significantly scatters electrons, inducing the deterioration of the electrical properties of the phototransistor. And it led to a weakened photoresponsivity than that of ZnO_{0.9}S_{0.1} [36]. In the case of ZnO_{0.9}S_{0.1}, the photoresponsivity was significantly improved than that of ZnO because of the decrease in the band gap and the increase in the number of oxygen vacancies, but the electrical properties deteriorated than that of ZnO. It can be also confirmed by the values shown in Table 1. The incorporation of S into ZnO led to an improvement of the photoresponsivity of the phototransistor, as well as the deterioration of the electrical properties.

To confirm the degree of enhancement of the photoresponsivity, the photoresponsivity and photosensitivity are calculated from the transfer curves, as shown in Fig. 4. The photoresponsivity of the phototransistors with the ZnO_{1-x}S_x active layer was calculated by the below equation according to the wavelengths (Fig. 4a). The V_D was 20 V, and the V_G was -15 V.

$$\text{Photoresponsivity} = \frac{(I_{\text{light}} - I_{\text{dark}}) / A_{\text{pt}}}{P / A_{\text{pd}}}$$

where I_{light} is the current of the phototransistors under illumination, I_{dark} is the dark current, A_{pt} is the product of the channel width and thickness, P is the power of the incident light, and A_{pd} is the spot size of the laser source. The phototransistor with ZnO showed a photoresponsivity of 4.9

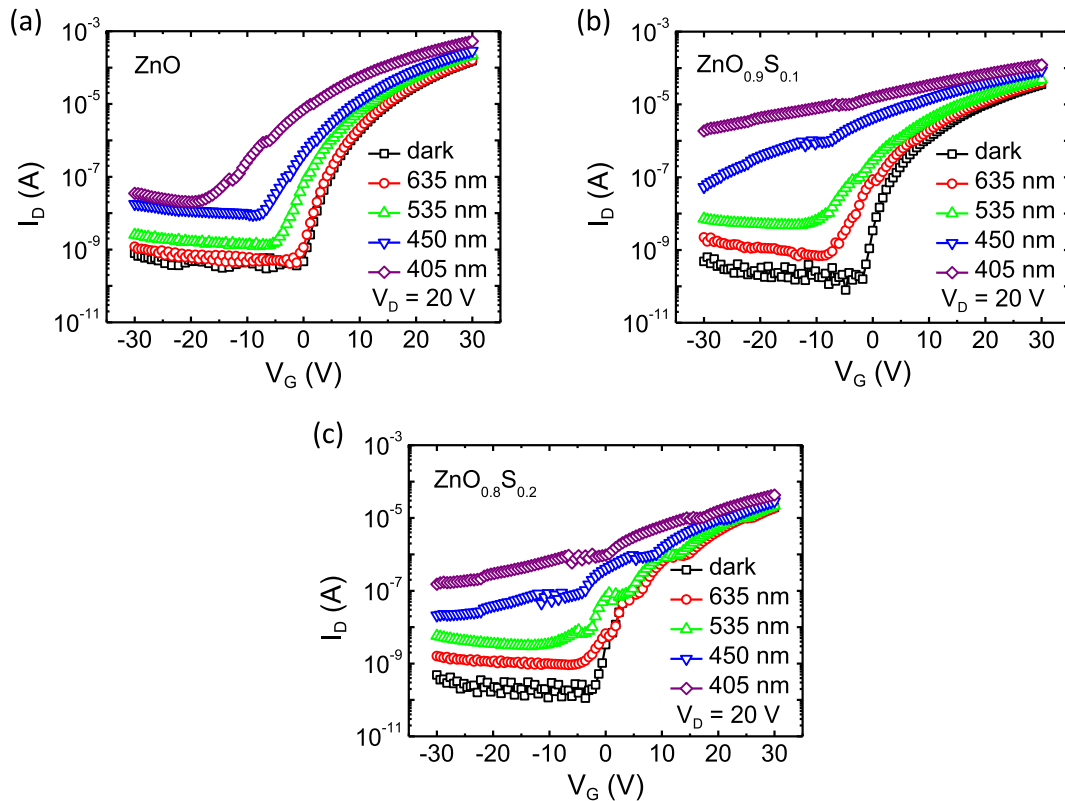


Fig. 3. (Color online) Transfer curves with the illumination of various wavelengths for (a) the phototransistor with ZnO, (b) the phototransistor with ZnO_{0.9}S_{0.1}, and (c) the phototransistor with ZnO_{0.8}S_{0.2}.

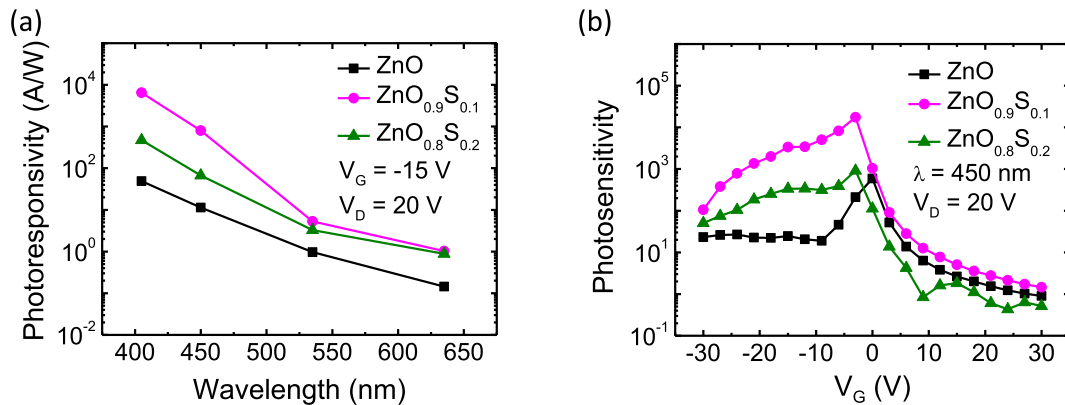


Fig. 4. (Color online) (a) Photoresponsivity of the phototransistors with ZnO_{1-x}S_x single active layer. (b) Photosensitivity of the phototransistors with ZnO_{1-x}S_x single active layer.

$\times 10$ A/W at a wavelength of 405 nm and 1.1×10 A/W at a wavelength of 450 nm. In addition, it had a very low photoresponsivity for the wavelength of 535 nm and 635 nm. In the case of ZnO_{0.9}S_{0.1}, the photoresponsivity was calculated as 6.5×10^3 A/W and 8.0×10^2 A/W for the wavelength of 405 nm and 450 nm, respectively. The photoresponsivity was significantly improved compared to the case of ZnO for the wavelength of 405 nm and 450 nm. Moreover, the photoresponsivity for the wavelength of 535 nm and 635 nm was also improved than that of ZnO. In the case of ZnO_{0.8}S_{0.2}, the photoresponsivity for the wavelength of 405 nm and 450 nm decreased to 4.7×10^2 A/W and 6.7×10 A/W compared to the case of ZnO_{0.9}S_{0.1}. However, the improved photoresponsivity was confirmed for all wavelengths of light as compared to the ZnO. The photosensitivity of the phototransistors with the ZnO_{1-x}S_x active layer was calculated by the below equation according to the

wavelengths (Fig. 4b). The photosensitivity is a unitless ratio of current. The V_D was 20 V, and the wavelength of the light was 450 nm. The light of 450 nm was selected to confirm the degree of the enhancement of the photosensitivity in the visible region.

$$\text{Photosensitivity} = \frac{(I_{\text{light}} - I_{\text{dark}})}{I_{\text{dark}}}$$

where I_{light} is the current of the phototransistors under illumination and I_{dark} is the dark current. In the case of ZnO, the maximum photosensitivity was 5.9×10^2 , whereas it considerably increased up to 1.7×10^4 in the case of ZnO_{0.9}S_{0.1}. In addition, photosensitivity increased in all ranges of V_G . Similar to the photoresponsivity trend, the photosensitivity of ZnO_{0.8}S_{0.2} was calculated to be the middle value between ZnO_{0.9}S_{0.1} and ZnO in the negative V_G region. The maximum photosensitivity was

9.2×10^2 . In the positive V_G region, the photosensitivity was lower than that of ZnO. It is because I_{light} significantly decreased due to the deterioration of the phototransistor with $\text{ZnO}_{0.8}\text{S}_{0.2}$, which can be confirmed in the positive V_G region of Fig. 3c. Thus, the composition of $\text{ZnO}_{1-x}\text{S}_x$ for the performance of the phototransistor was optimized for $\text{ZnO}_{0.9}\text{S}_{0.1}$.

To identify the differences in the characteristics of photoresponsivity and photosensitivity according to the wavelength, the chemical state of $\text{ZnO}_{1-x}\text{S}_x$ as a function of S content was analyzed by measuring XPS. In the S 2p spectra, as the amount of S increased, the intensity of the S 2p peak increased at 161.9 eV, which did not exist in the case of ZnO. In the Zn 2p_{3/2} spectra, as the amount of S increased, a peak shift was observed from 1021.6 eV to 1021.8 eV, which is due to the increase of Zn-S bonding with higher binding energy than Zn-O bonding in proportion to the S content in the film (refer to Supporting Fig. S2) [51,52]. To extract the chemical states related to oxygen vacancies in the $\text{ZnO}_{1-x}\text{S}_x$ film, the O 1s spectra is deconvoluted, as shown in Fig. 5. There were three phases, with peak positions of 530.4 eV, 531.7 eV, and 532.6 eV, marked as O_I, O_{II}, and O_{III}. O_I is ascribed to Zn-O bonding, O_{II} corresponds to the oxygen vacancy, and O_{III} reflects the hydroxyl group of $\text{ZnO}_{1-x}\text{S}_x$ [32,53]. The relative area ratio is obtained from each O 1s peak depending on the S content in the $\text{ZnO}_{1-x}\text{S}_x$ film, as indicated in Fig. 5b. It was clear that when the amount of S increased, the O_I corresponding to the Zn-O bonding decreased and the O_{II} corresponding to the oxygen vacancy increased. However, there was no significant difference in O_{III} corresponding to the hydroxyl group. The trend of oxygen vacancies in $\text{ZnO}_{1-x}\text{S}_x$ was the same as the device performance. Oxygen vacancies formed at sub-gaps leads to the flow of photocurrent even with the light of low energy, which allows the improvement of the photoresponsivity, as shown in Fig. 3. However, too much S in the ZnO lattice significantly scatters electrons. It led to the deteriorated electrical properties and poor performance of the phototransistor with $\text{ZnO}_{0.8}\text{S}_{0.2}$.

To understand the mechanism of the movement of electrons in the phototransistor with the $\text{ZnO}_{1-x}\text{S}_x$ active layer in terms of photoresponsivity, we attempted to depict the band diagram of $\text{ZnO}_{1-x}\text{S}_x$ in contact with a SiO₂ gate oxide by measuring XPS. The extrapolation technique was used for the valence band spectra of $\text{ZnO}_{1-x}\text{S}_x$ as a function of S content. From the results, each ΔE_V ($\Delta E_V = E_F - E_V$) was characterized by 2.79 eV, 2.55 eV, and 1.99 eV for ZnO, $\text{ZnO}_{0.9}\text{S}_{0.1}$, and

$\text{ZnO}_{0.8}\text{S}_{0.2}$, respectively (refer to Supporting Fig. S3). Based on the band gap obtained from the tauc plot (Fig. 1b), each ΔE_C ($\Delta E_C = E_C - E_F$) was calculated by 0.45 eV, 0.60 eV, and 0.97 eV for ZnO, $\text{ZnO}_{0.9}\text{S}_{0.1}$, and $\text{ZnO}_{0.8}\text{S}_{0.2}$, respectively. The energy band diagrams of the phototransistors with the $\text{ZnO}_{1-x}\text{S}_x$ active layer were obtained by synthesizing the above factors. As the amount of S increased, the conduction band minimum (CBM) was further away from the Fermi level (E_F) in the $\text{ZnO}_{1-x}\text{S}_x$ layer. It means that the electrical conductivity decreased as the amount of S increased in the $\text{ZnO}_{1-x}\text{S}_x$ film, which influenced the electrical properties of the phototransistors. It is revealed that the transfer curve become unstable as the amount of S increases, as shown in Fig. 2b. In ZnO, higher defect density generally means higher carrier concentration, which increases the electrical conductivity of the film. It means the narrowing between the E_F and the CBM. However, as the composition of S increased, the electron mobility of the film decreased significantly due to the interference of the S atom with electron movement. The electrical conductivity is affected by both carrier concentration and electron mobility. As a result, according to the increase of S content, the electrical conductivity of the film decreased due to the deteriorated electron mobility. It means a wider gap between the E_F and the CBM. We observe that the difference in the photoresponsivity gets larger when the V_G is negative in the phototransistor, as shown in Fig. 3, which induces upward band bending of the $\text{ZnO}_{1-x}\text{S}_x$ layer [20,23].

Based on the chemical states and energy band diagram, we propose a mechanism for the movement of electrons in the phototransistors with a $\text{ZnO}_{1-x}\text{S}_x$ active layer, as described in Fig. 6 [14,20,23,39–41]. The photoresponsivity showed the highest value with irradiation at a wavelength of 405 nm (Fig. 4a). According to the literature, oxygen vacancies exist as sub-gap states [44–46]. And ionized oxygen vacancies act as donors to donate electrons in the $\text{ZnO}_{1-x}\text{S}_x$ film when light with sufficiently high energy is irradiated [47,48]. These oxygen vacancies become larger at the sub-gap of the $\text{ZnO}_{1-x}\text{S}_x$ film with increasing S content [49,50]. When light with sufficiently high energy is injected into the $\text{ZnO}_{1-x}\text{S}_x$ film, the number of electrons excited to the conduction band increases in proportion to the S content because of the reduced band gap of the $\text{ZnO}_{1-x}\text{S}_x$ film and the increased number of oxygen vacancies. At negative V_G , electrons migrate to the surface and then flow between the Al source and drain. However, even though the number of

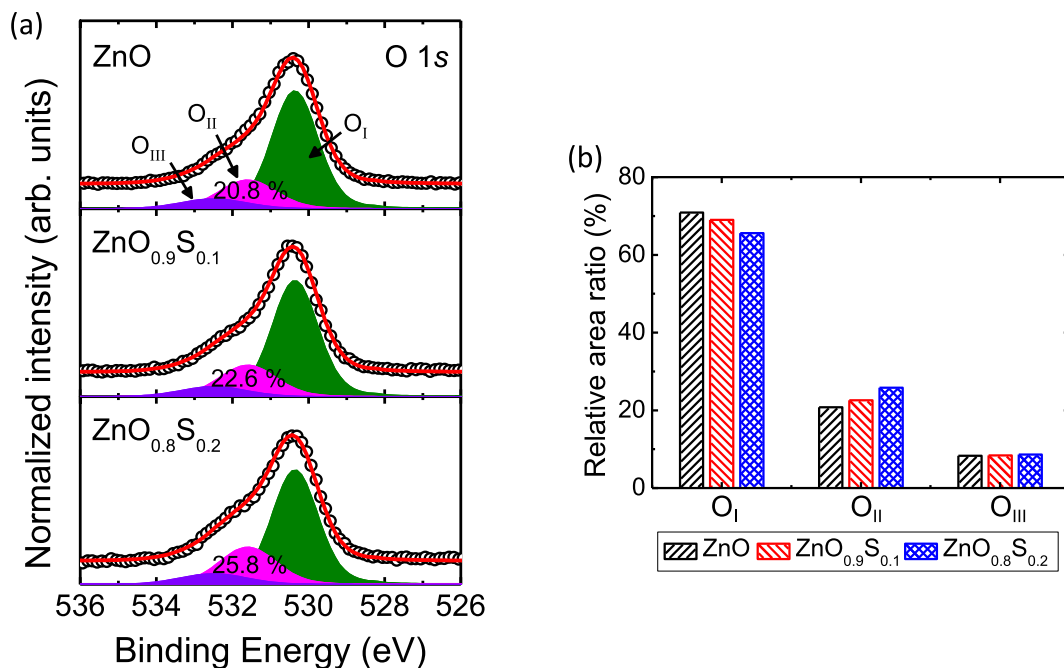


Fig. 5. (Color online) (a) Deconvoluted result of XPS O 1s spectra of $\text{ZnO}_{1-x}\text{S}_x$. (b) Ratio of the three peaks (O_I, O_{II}, and O_{III}) area in the deconvoluted result of XPS O 1s spectra of $\text{ZnO}_{1-x}\text{S}_x$.

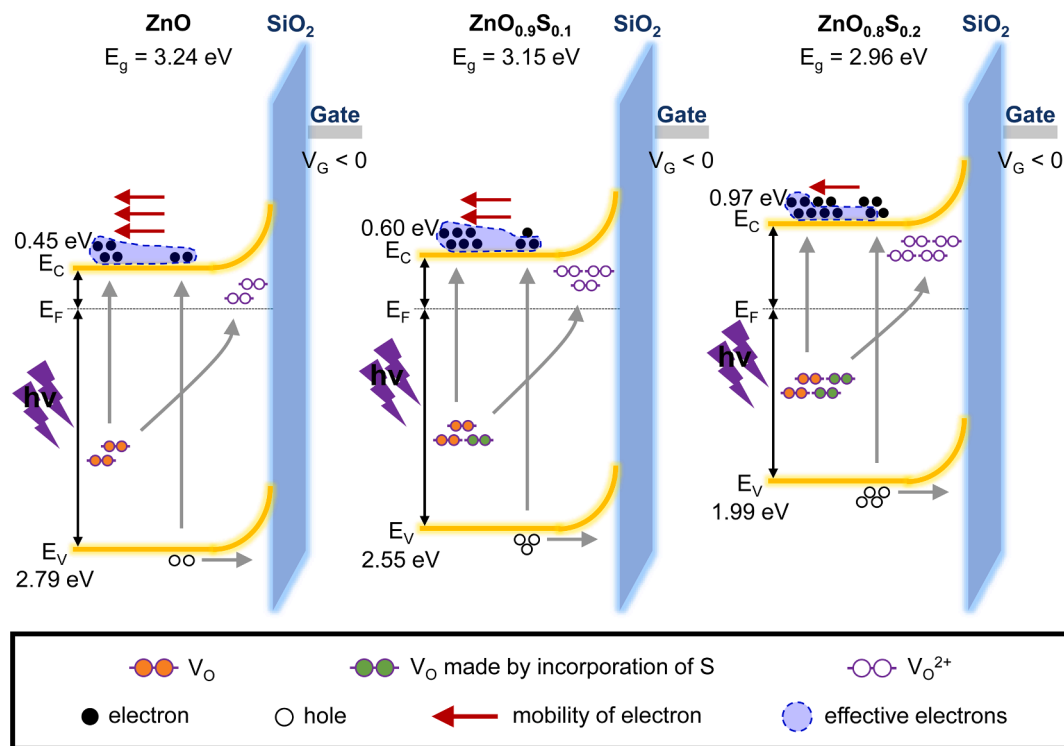


Fig. 6. (Color online) Energy band diagrams of the phototransistors with $\text{ZnO}_{1-x}\text{S}_x$ single active layer.

excited electrons is larger, if the electron mobility is too low, the number of electrons contributing to the current becomes small. Thus, the current flow is determined by the effective electrons governed by both the number of electrons and the mobility. Because the photoresponsivity is determined by the effective electrons, it is reasonable that photoresponsivity showed the best performance in the case of $\text{ZnO}_{0.9}\text{S}_{0.1}$.

4. Conclusions

We applied $\text{ZnO}_{1-x}\text{S}_x$ with electrical tunability to a phototransistor as a single active layer. As the amount of S increased, the band gap of $\text{ZnO}_{1-x}\text{S}_x$ decreased, and the electrical characteristics of the transistor, such as electron saturation mobility and on-off ratio, deteriorated. However, the incorporation of S enhanced the photoresponsivity of the phototransistor in the UV and visible regions, especially for the wavelength of 405 nm and 450 nm. The phototransistor with $\text{ZnO}_{0.9}\text{S}_{0.1}$ showed photoresponsivity and maximum photosensitivity of 8.0×10^2 A/W and 1.7×10^4 , for the wavelength of 450 nm. Through XPS measurements, it was confirmed that the cause of the improvement of the photoresponsivity was originated from the increase of the number of oxygen vacancies. In addition, the mechanism of electron transport in the phototransistors with the $\text{ZnO}_{1-x}\text{S}_x$ single active layer was demonstrated by the energy band diagrams derived from XPS analysis. Consequently, our results suggest that the $\text{ZnO}_{1-x}\text{S}_x$ single active layer successfully improved the photoresponsivity of the phototransistors in the UV and visible regions.

CRedit authorship contribution statement

Jong Hun Yu: Conceptualization, Methodology, Formal analysis, Writing – original draft. **Woo-Jung Lee:** Methodology, Formal analysis, Writing – original draft. **Dae-Hyung Cho:** Methodology, Formal analysis, Resources. **Woo-Ju Kim:** Resources, Data curation. **Seong Jun Kang:** Investigation, Supervision, Writing – review & editing. **Yong-Duck Chung:** Investigation, Supervision, Writing – review & editing.

Declaration of Competing Interest

The authors declare that they have no known competing financial interests or personal relationships that could have appeared to influence the work reported in this paper.

Acknowledgments

This work was supported by Electronics and Telecommunications Research Institute (ETRI) grant funded by the Korean government [21YB2200, 21YB2900] and this study was supported by a research project grant from the NRF of Korea (2021R1A2C1009442).

Appendix A. Supplementary material

Supplementary data to this article can be found online at <https://doi.org/10.1016/j.apsusc.2022.153062>.

References

- [1] A.M. Ortiz, D. Hussein, S. Park, S.N. Han, N. Crespi, The cluster between internet of things and social networks: Review and research challenges, *IEEE Internet Things J.* 1 (3) (2014) 206–215, <https://doi.org/10.1109/JIOT.2014.2318835>.
- [2] F. Wortmann, K. Flüchter, Internet of things, *Bus. Inf. Syst. Eng.* 57 (2015) 221–224, <https://doi.org/10.1007/s12599-015-0383-3>.
- [3] A.-M. Cailean, M. Dimian, A. Done, Enhanced design of visible light communication sensor for automotive applications: Experimental demonstration of a 130 meters link, *IEEE*, 2018, pp. 1–4, <https://doi.org/10.23919/GLC.2018.8319100>.
- [4] R. Raskar, P. Beardsley, J. van Baar, Y. Wang, P. Dietz, J. Lee, D. Leigh, T. Willwacher, RFIG lamps: Interacting with a self-describing world via photosensing wireless tags and projectors, in: *ACM SIGGRAPH 2004 Papers* 23 (3) (2004) 406–415, <https://doi.org/10.1145/1015706.1015738>.
- [5] J. Gubbi, R. Buyya, S. Marusic, M. Palaniswami, Internet of Things (IoT): A vision, architectural elements, and future directions, *Futur. Gener. Comp. Syst.* 29 (7) (2013) 1645–1660, <https://doi.org/10.1016/j.future.2013.01.010>.
- [6] A.K. Sikder, G. Petracca, H. Aksu, T. Jaeger, A.S. Uluagac, A survey on sensor-based threats to internet-of-things (IoT) devices and applications, *arXiv preprint arXiv:1802.02041*, (2018), doi: 10.48550/arXiv.1802.02041.

- [7] M.M. Nezhad, M. Eshghi, Sensor single and multiple anomaly detection in wireless sensor networks for healthcare, in: 2019 27th Iranian Conference on Electrical Engineering (ICEE), 2019, pp. 1751–1755.
- [8] K. Nomura, H. Ohta, A. Takagi, T. Kamiya, M. Hirano, H. Hosono, Room-temperature fabrication of transparent flexible thin-film transistors using amorphous oxide semiconductors, *Nature* 432 (2004) 488–492, <https://doi.org/10.1038/nature03090>.
- [9] M. Kim, J.H. Jeong, H.J. Lee, T.K. Ahn, H.S. Shin, J.-S. Park, J.K. Jeong, Y.-G. Mo, H.D. Kim, High mobility bottom gate InGaZnO thin film transistors with SiO_x etch stopper, *Appl. Phys. Lett.* 90 (2007), 212114, <https://doi.org/10.1063/1.2742790>.
- [10] J.-S. Park, J.K. Jeong, Y.-G. Mo, H.D. Kim, S.-I. Kim, Improvements in the device characteristics of amorphous indium gallium zinc oxide thin-film transistors by Ar plasma treatment, *Appl. Phys. Lett.* 90 (2007), 262106, <https://doi.org/10.1063/1.2753107>.
- [11] R.B.M. Cross, M.M. De Souza, Investigating the stability of zinc oxide thin film transistors, *Appl. Phys. Lett.* 89 (26) (2006) 263513, <https://doi.org/10.1063/1.2425020>.
- [12] T. Hirao, M. Furuta, H. Furuta, T. Matsuda, T. Hiramatsu, H. Hokari, M. Yoshida, H. Ishii, M. Kakegawa, Novel top-gate zinc oxide thin-film transistors (ZnO TFTs) for AMLCDs, *J. Soc. Inf. Display* 15 (1) (2007) 17, <https://doi.org/10.1889/1.2451545>.
- [13] K. Park, D.-K. Lee, B.-S. Kim, H. Jeon, N.-E. Lee, D. Whang, H.-J. Lee, Y.J. Kim, J.-H. Ahn, Stretchable, transparent zinc oxide thin film transistors, *Adv. Funct. Mater.* 20 (20) (2010) 3577–3582, <https://doi.org/10.1002/adfm.201001107>.
- [14] B.J. Kim, S. Park, T.Y. Kim, E.Y. Jung, J.-A. Hong, B.-S. Kim, W. Jeon, Y. Park, S. J. Kang, Improving the photoresponsivity and reducing the persistent photocurrent effect of visible-light ZnO/quantum-dot phototransistors via a TiO₂ layer, *J. Mater. Chem. C* 8 (46) (2020) 16384–16391, <https://doi.org/10.1039/D0TC03353G>.
- [15] E.M.C. Fortunato, P.M.C. Barquinha, A.C.M.B.G. Pimentel, A.M.F. Gonçalves, A.J. S. Marques, R.F.P. Martins, L.M.N. Pereira, Wide-bandgap high-mobility ZnO thin-film transistors produced at room temperature, *Appl. Phys. Lett.* 85 (13) (2004) 2541–2543, <https://doi.org/10.1063/1.1790587>.
- [16] Y.S. Rim, K.-C. Ok, Y.M. Yang, H. Chen, S.-H. Bae, C. Wang, Y.u. Huang, J.-S. Park, Y. Yang, Boosting responsivity of organic-metal oxynitride hybrid heterointerface phototransistor, *ACS Appl. Mater. Interfaces* 8 (23) (2016) 14665–14670, <https://doi.org/10.1021/acsami.6b02814>.
- [17] J. Yu, B.J. Kim, S. Park, I.K. Han, S.J. Kang, Red/green/blue selective phototransistors with a hybrid structure of quantum-dots and an oxide semiconductor, *Jpn. J. Appl. Phys.* 57 (4) (2018) 044001, <https://doi.org/10.7567/JJAP.57.044001>.
- [18] Y. Zhai, G. Chen, J. Ji, Z. Wu, Y. Li, Q. Wang, Investigation of photocurrent transient variation in Au nanoparticles-decorated IGZO phototransistor, *Physica E: Low-Dimens. Syst. Nanostruct.* 113 (2019) 92–96, <https://doi.org/10.1016/j.physe.2019.04.003>.
- [19] Y.-H. Lin, H. Faber, J.G. Labram, E. Stratakis, L. Sygellou, E. Kymakis, N.A. Hastas, R. Li, K. Zhao, A. Amassian, N.D. Treat, M. McLachlan, T.D. Anthopoulos, High Electron mobility thin-film transistors based on solution-processed semiconducting metal oxide heterojunctions and quasi-superlattices, *Adv. Sci.* 2 (7) (2015) 1500058, <https://doi.org/10.1002/advs.201500058>.
- [20] J. Chung, Y.J. Tak, W.-G. Kim, B.H. Kang, H.J. Kim, Artificially fabricated subgap states for visible-light absorption in indium-gallium-zinc oxide phototransistor with solution-processed oxide absorption layer, *ACS Appl. Mater. Interfaces* 11 (42) (2019) 38964–38972, <https://doi.org/10.1021/acsami.9b14154>.
- [21] T. Kim, J. Hur, S. Jeon, The influence of interfacial defects on fast charge trapping in nanocrystalline oxide-semiconductor thin film transistors, *Semicond. Sci. Technol.* 31 (5) (2016) 055014, <https://doi.org/10.1088/0268-1242/31/5/055014>.
- [22] M.G. Yun, Y.K. Kim, C.H. Ahn, S.W. Cho, W.J. Kang, H.K. Cho, Y.-H. Kim, Low voltage-driven oxide phototransistors with fast recovery, high signal-to-noise ratio, and high responsivity fabricated via a simple defect-generating process, *Sci. Rep.* 6 (2016) 1–9, <https://doi.org/10.1038/srep31991>.
- [23] Y.J. Tak, D.J. Kim, W.-G. Kim, J.H. Lee, S.J. Kim, J.H. Kim, H.J. Kim, Boosting visible light absorption of metal-oxide-based phototransistors via heterogeneous In-Ga-Zn-O and CH₃NH₃PbI₃ films, *ACS Appl. Mater. Interfaces* 10 (15) (2018) 12854–12861, <https://doi.org/10.1021/acsami.8b01427>.
- [24] J. Yu, S.W. Shin, K.-H. Lee, J.-S. Park, S.J. Kang, Visible-light phototransistors based on InGaZnO and silver nanoparticles, *J. Vac. Sci. Technol. B* 33 (6) (2015) 061211, <https://doi.org/10.1116/1.4936113>.
- [25] P. Sinsersuksakul, K. Hartman, S. Bok Kim, J. Heo, L. Sun, H. Hejin Park, R. Chakraborty, T. Buonassisi, R.G. Gordon, Enhancing the efficiency of SnS solar cells via band-offset engineering with a zinc oxysulfide buffer layer, *Appl. Phys. Lett.* 102 (5) (2013) 053901, <https://doi.org/10.1063/1.4789855>.
- [26] R.L. Garris, J.V. Li, M.A. Contreras, K. Ramanathan, L.M. Mansfield, B. Egaas, A. Kanevce, Efficient and stable CIGS solar cells with ZnOS buffer layer, *IEEE*, 2014, pp. 0353–0356, <https://doi.org/10.1109/PVSC.2014.6924930>.
- [27] T.-M. Hsieh, S.J. Lue, J. Ao, Y. Sun, W.-S. Feng, L.-B. Chang, Characterizations of chemical bath-deposited zinc oxysulfide films and the effects of their annealing on copper-indium-gallium-selenide solar cell efficiency, *J. Power Sources* 246 (2014) 443–448, <https://doi.org/10.1016/j.jpowsour.2013.07.090>.
- [28] T. Minemoto, A. Okamoto, H. Takakura, Sputtered ZnO-based buffer layer for band offset control in Cu(In,Ga)Se₂ solar cells, *Thin Solid Films* 519 (21) (2011) 7568–7571, <https://doi.org/10.1016/j.tsf.2010.12.117>.
- [29] J.-H. Wi, T.G. Kim, J.W. Kim, W.-J. Lee, D.-H. Cho, W.S. Han, Y.-D. Chung, Photovoltaic performance and interface behaviors of Cu(In,Ga)Se₂ solar cells with a sputtered-Zn(O,S) buffer layer by high-temperature annealing, *ACS Appl. Mater. Interfaces* 7 (31) (2015) 17425–17432, <https://doi.org/10.1021/acsami.5b04815>.
- [30] D.-H. Cho, W.-J. Lee, M.-E. Kim, B. Shin, Y.-D. Chung, Color tuning in Cu(In,Ga)Se₂ thin-film solar cells by controlling optical interference in transparent front layers, *Prog. Photovoltaics* 28 (8) (2020) 798–807, <https://doi.org/10.1002/pip.3272>.
- [31] W.-J. Lee, D.-H. Cho, J.M. Bae, M.E. Kim, J. Park, Y.-D. Chung, Ultrafast wavelength-dependent carrier dynamics related to metastable defects in Cu(In,Ga)Se₂ solar cells with chemically deposited Zn(O,S) buffer layer, *Nano Energy* 74 (2020), 104855, <https://doi.org/10.1016/j.nanoen.2020.104855>.
- [32] D.-H. Cho, W.-J. Lee, B. Shin, Y.-D. Chung, Analysis of vertical phase distribution in reactively sputtered zinc oxysulfide thin films, *Appl. Surf. Sci.* 486 (2019) 555–560, <https://doi.org/10.1016/j.apsusc.2019.04.200>.
- [33] D.-H. Cho, W.-J. Lee, M.E. Kim, K. Kim, J.H. Yun, Y.-D. Chung, Reactively sputtered Zn(O,S) buffer layers for controlling band alignment of Cu(In,Ga)Se₂ thin-film solar cell interface, *J. Alloy. Compd.* 842 (2020), 155986, <https://doi.org/10.1016/j.jallcom.2020.155986>.
- [34] J. Kim, J. Kim, E. Ko, H.K. Park, S. Yoon, D.-H. Cho, W.-J. Lee, Y.-D. Chung, W. Jo, Unraveling interface characteristics of Zn(O,S)/Cu(In,Ga)Se₂ at nanoscale: Enhanced hole transport by tuning band offsets, *Appl. Surf. Sci.* 509 (2020), 144782, <https://doi.org/10.1016/j.apsusc.2019.144782>.
- [35] B. Meyer, A. Polity, B. Farangis, Y. He, D. Hasselkamp, T. Krämer, C. Wang, Structural properties and bandgap bowing of ZnO_{1-x}S_x thin films deposited by reactive sputtering, *Appl. Phys. Lett.* 85 (2004) 4929–4931, <https://doi.org/10.1063/1.1825053>.
- [36] H. Pan, T. Yang, B. Yao, R. Deng, R. Sui, L. Gao, D. Shen, Characterization and properties of ZnO_{1-x}S_x alloy films fabricated by radio-frequency magnetron sputtering, *Appl. Surf. Sci.* 256 (2010) 4621–4625, <https://doi.org/10.1016/j.apsusc.2010.02.061>.
- [37] C. Persson, C. Platzer-Björkman, J. Malmström, T. Törndahl, M. Edoff, Strong valence-band offset bowing of ZnO_{1-x}S_x enhances p-type nitrogen doping of ZnO-like alloys, *Phys. Rev. Lett.* 97 (2006), 146403, <https://doi.org/10.1103/PhysRevLett.97.146403>.
- [38] V. Khomyak, I. Shteplyuk, V. Khranovskyy, R. Yakimova, Band-gap engineering of ZnO_{1-x}S_x films grown by rf magnetron sputtering of ZnS target, *Vacuum* 121 (2015) 120–124, <https://doi.org/10.1016/j.vacuum.2015.08.008>.
- [39] B.J. Kim, N.-K. Cho, S. Park, S. Jeong, D. Jeon, Y. Kang, T. Kim, Y.S. Kim, I.K. Han, S.J. Kang, Highly transparent phototransistor based on quantum-dots and ZnO bilayers for optical logic gate operation in visible-light, *RSC Adv.* 10 (2020) 16404–16414, <https://doi.org/10.1039/D0RA01756F>.
- [40] B.J. Kim, J.H. Jeong, E.Y. Jung, T.Y. Kim, S. Park, J.-A. Hong, K.-M. Lee, W. Jeon, Y. Park, S.J. Kang, A visible-light phototransistor based on the heterostructure of ZnO and TiO₂ with trap-assisted photocurrent generation, *RSC Adv.* 11 (2021) 12051–12057, <https://doi.org/10.1039/D1RA00801C>.
- [41] S. Park, B.J. Kim, T.Y. Kim, E.Y. Jung, K.-M. Lee, J.-A. Hong, W. Jeon, Y. Park, S. J. Kang, Improving the photodetection and stability of a visible-light QDs/ZnO phototransistor via an Al₂O₃ additional layer, *J. Mater. Chem. C* 9 (7) (2021) 2550–2560, <https://doi.org/10.1039/D0TC05626J>.
- [42] M. Mativenga, S. An, J. Jang, Bulk accumulation a-IGZO TFT for high current and turn-on voltage uniformity, *IEEE Electron Device Lett.* 34 (12) (2013) 1533–1535, <https://doi.org/10.1109/LED.2013.2284599>.
- [43] X. Li, D.i. Geng, M. Mativenga, J. Jang, High-speed dual-gate a-IGZO TFT-based circuits with top-gate offset structure, *IEEE Electron Device Lett.* 35 (4) (2014) 461–463, <https://doi.org/10.1109/LED.2014.2305665>.
- [44] F. Oba, S.R. Nishitani, S. Isotani, H. Adachi, I. Tanaka, Energetics of native defects in ZnO, *J. Appl. Phys.* 90 (2) (2001) 824–828, <https://doi.org/10.1063/1.1380994>.
- [45] D.M. Hofmann, D. Pfisterer, J. Sann, B.K. Meyer, R. Tena-Zaera, V. Munoz-Sanjose, T. Frank, G. Pensl, Properties of the oxygen vacancy in ZnO, *Appl. Phys. A* 88 (1) (2007) 147–151, <https://doi.org/10.1007/s00339-007-3956-2>.
- [46] F. Selim, M. Weber, D. Solodovnikov, K. Lynn, Nature of native defects in ZnO, *Phys. Rev. Lett.* 99 (2007), 085502, <https://doi.org/10.1103/PhysRevLett.99.085502>.
- [47] A. Janotti, C.G. Van de Walle, Oxygen vacancies in ZnO, *Appl. Phys. Lett.* 87 (12) (2005) 122102, <https://doi.org/10.1063/1.2053360>.
- [48] A. Janotti, C.G. Van de Walle, New insights into the role of native point defects in ZnO, *J. Cryst. Growth* 287 (2006) 58–65, <https://doi.org/10.1016/j.jcrysgro.2005.10.043>.
- [49] A.B. Patil, K.R. Patil, S.K. Pardeshi, Ecofriendly synthesis and solar photocatalytic activity of S-doped ZnO, *J. Hazard. Mater.* 183 (2010) 315–323, <https://doi.org/10.1016/j.jhazmat.2010.07.026>.
- [50] M.A. Awad, E.M.M. Ibrahim, A.M. Ahmed, One step syntheses of S incorporated ZnO nanowires for photocatalysis applications, *Eur. Phys. J. Appl. Phys.* 72 (2015) 30303, <https://doi.org/10.1051/epjap/2015150257>.
- [51] V. Kumari, A. Mittal, J. Jindal, S. Yadav, N. Kumar, S.-N. and C-doped ZnO as semiconductor photocatalysts: A review, *Front. Mater. Sci.* 13 (1) (2019) 1–22, <https://doi.org/10.1007/s11706-019-0453-4>.
- [52] L. Li, M.i. Zhang, Q. Wang, P. Li, M. Li, Y. Lu, H. Chen, Y. He, The band alignment of nonpolar m-plane ZnO_{1-x}S_x/Mg_{0.4}Zn_{0.6}O heterojunctions, *AIP Adv.* 10 (1) (2020) 015314, <https://doi.org/10.1063/1.5093025>.
- [53] K.S. Ranjith, A. Senthambizhan, B. Balusamy, T. Uyar, Nanografted surface shell wall controlled ZnO-ZnS core-shell nanofibers and their shell wall thickness dependent visible photocatalytic properties, *Catal. Sci. Technol.* 7 (5) (2017) 1167–1180, <https://doi.org/10.1039/C6CY02556K>.